Letter | Editors' Suggestion

Gate-tunable heavy fermion quantum criticality in a moiré Kondo lattice

Ajesh Kumar,[1,*] Nai Chao Hu,[1,*] Allan H. MacDonald,[1] and Andrew C. Potter[1,2]
[1]*Department of Physics, University of Texas at Austin, Austin, Texas 78712, USA*
[2]*Department of Physics, University of British Columbia, Vancouver, British Columbia V6T 1Z1, Canada*

(Received 6 December 2021; revised 4 April 2022; accepted 8 July 2022; published 27 July 2022)

We propose a realization of Kondo lattice physics in moiré superlattices at the interface between a WX_2 homobilayer and MoX_2 monolayer ($X = S, Se$). Under appropriate gating conditions, the interface WX_2 layer forms a triangular lattice of local moments that couple to itinerant electrons in the other WX_2 layer via a gate-tunable Kondo exchange interaction. Using a parton mean-field approach, we identify a range of twist angles which support a gate-tuned quantum phase transition between a heavy Fermi liquid with large anomalous Hall conductance and a chiral spin liquid coexisting with a light Fermi liquid and describe experimental signatures to distinguish among competing theoretical scenarios.

DOI: 10.1103/PhysRevB.106.L041116

Crystals containing lanthanide or actinide elements host f-electron local spin moments coupled via Kondo spin-exchange interactions to itinerant conduction (c) electrons. The phase diagrams of such Kondo lattice systems are often extremely rich and can include magnetic and nonmagnetic states, superconductors, and non-Fermi liquids [1–5]. When Kondo-screening effects dominate, the f spins hybridize with c electrons and contribute to the Luttinger volume of the Fermi sea producing exceptionally high (heavy fermion) quasiparticle masses [1–3] arising from the narrow f bandwidth. Alternatively, dominant spin-spin interactions [chiefly c mediated by Ruderman-Kittel-Kasuya-Yosida (RKKY) coupling] cause f local moments to order into either (i) a magnetic state [6], which is typically an antiferromagnet (AFM), or (ii) a quantum spin liquid (QSL) [5,7], if magnetic order is frustrated.

These Kondo-(un)screened phases are separated by a quantum critical point marked by a fan of non-Fermi-liquid transport signatures [2–4,8] that is often partly occluded by an unconventional superconducting dome. The hallmark of this apparently continuous critical point is a sudden change in the size of the Fermi surface. Understanding the nature of such Fermi-volume-changing transitions and their relation to non-Fermi-liquid behavior is thought to be key to understanding many other strongly correlated systems such as high-temperature cuprate superconductors, and remains a key unsolved problem in condensed-matter physics. Moreover, different experiments and theoretical analyses produce a conflicting picture of the nature of the nonhybridized phase, and its nature remains hotly debated despite decades of intensive study. The complex microscopic structure and many-band character of f-electron materials along with the limited ability to tune carrier densities and exchanging couplings in bulk three-dimensional (3D) crystals pose significant obstacles to resolving these mysteries.

In this Research Letter we propose that progress can be achieved by using recently discovered transition metal dichalcogenide (TMD) moiré material platforms to construct a synthetic Kondo lattice made from relatively simple well-understood components. Crucially, we will show that the Kondo exchange coupling can be continuously tuned by electrostatic gate tuning, enabling *in situ* access to the entire heavy fermion phase diagram and criticality in a single device. Furthermore, these systems have triangular-lattice symmetries that tend to frustrate magnetic order and can favor fractionalized QSL states. Our main results are summarized in Fig. 1, which contains phase diagrams in the two-dimensional gate-voltage phase space of dual-gated two-dimensional materials. We first identify the twist-angle-dependent area within which a Kondo lattice model is realized and then estimate the location of the Kondo-screening quantum critical line. Parton mean-field calculations predict a quantum criticality scenario in which local moments in a weak-coupling chiral spin liquid (CSL) state hybridize with conduction electrons to form a strong-coupling heavy Fermi liquid that exhibits an anomalous Hall effect. Previous works on the triangular-Kondo-lattice model [9,10] support the existence of such anomalous Hall states due to nonzero spin chirality. The parton mean-field approach used here should be viewed as a way to obtain a regime where quantum criticality is likely to occur. We discuss experimental probes of Kondo lattice physics in moiré materials that discriminate among various competing AFM and QSL weak-Kondo-coupling scenarios, including the ones not favored by the parton mean-field theory, highlighting electrical and thermal Hall transport and electrostatic measurements of entropy. Compared with previous proposals for achieving heavy fermion physics in moiré systems, our setup directly implements a Kondo lattice model using already-demonstrated moiré ingredients; it avoids both topological obstacles [11–14] to local-moment physics of proposed twisted graphene multilayer realizations [15] and the need for unusual spontaneous orbital selectivity required to form local moments in electron-doped TMD heterobilayers [16].

*These authors contributed equally to this work.

 ©2022 American Physical Society

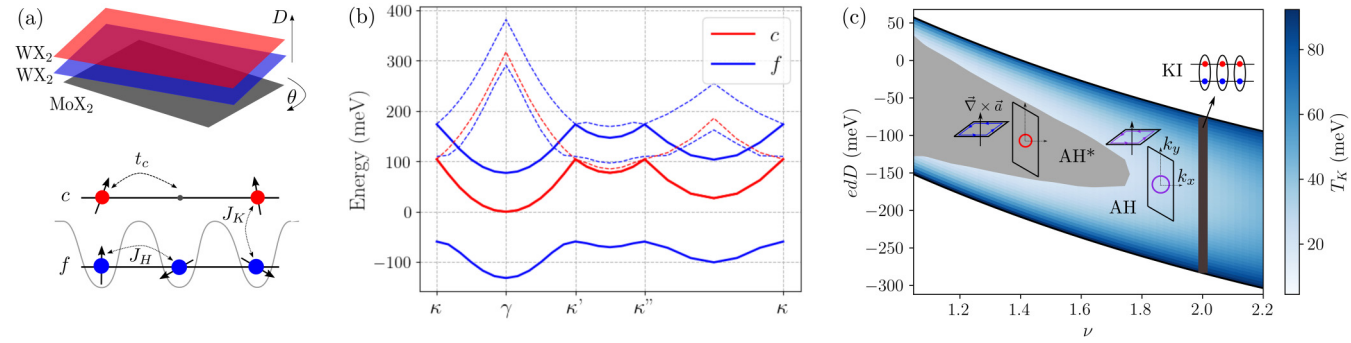

FIG. 1. Kondo lattice simulator. (a) Schematic of a TMD trilayer Kondo lattice system. The two active TMD layers experience moiré modulation potentials with different strengths so that one layer has flat bands and one has dispersive bands. When the density in the flat-band layer is tuned to one electron per moiré period and the total density is tuned to a higher value, a triangular-lattice Kondo model is realized. (b) Gated self-consistent Hartree-Fock band structures in the middle of the Kondo lattice model regime at $\theta = 4.5^\circ$, with filling factors $\nu_f = 1$ and $\nu_c = 0$. The solid blue bands are the upper and lower Hubbard bands in the f layer. The dashed blue bands are the second lowest energy f band in each spin. The red bands are the lowest (solid curves) and second lowest (dashed curves) energy (spin-degenerate) bands in the c layer with bandwidth 104.49 meV. (c) Parton mean-field phase diagram as a function of the moiré band filling factor ν and the external displacement field D (edD), which are linearly related to the top and bottom gate voltages. The black lines bound the Kondo lattice regime, within which the mean-field filling factor is 1 in the f layer and $\nu_c = \nu - 1$ in the c layer. In the AH* phase, a Fermi surface of c electrons (red) is decoupled from a chiral spin liquid (CSL) of spinons f. In the AH phase the Fermi surface (purple) has mixed c and f character. The Kondo insulator (KI) phase at $\nu = 2$ is adiabatically connected to the direct product of singlets between c and f electrons on each site. The color scale indicates the Kondo temperature of the AH states.

A synthetic Kondo lattice. We propose a realization of Kondo lattice physics in TMD trilayers in which a triangular-lattice moiré pattern is formed between an atomically aligned WX_2 bilayer twisted by a small angle θ relative to an MoX_2 monolayer, where $X = S, Se$ is a chalcogen. We note that one could alternatively form a moiré potential by choosing different chalcogens for the WX_2 and MoX_2 layers to force a lattice mismatch (though we do not model that case here). The active valence-band degrees of freedom reside in the WX_2 layers and come from momenta near the K and K' points [17] in the triangular-lattice Brillouin zone, where strong spin-orbit coupling locks the spin and valley degrees of freedom into a single effective spin-$\frac{1}{2}$ moment (with approximate SU(2)-symmetric interactions [18,19]) that we will refer to simply as spin. Because the bottom WX_2 layer (closest to the MoX_2) experiences a stronger moiré modulation potential [19], its triangular-lattice symmetric moiré minibands will be narrower, enhancing correlations in this layer. Temporarily neglecting interlayer tunneling, the goal will be to half-fill the lowest moiré miniband of the lower (f) layer to form a Mott insulator of well-formed local moments, and partially fill the upper layer (c) to form a conducting Fermi surface. Mott insulators in related TMD bilayers have been achieved in several recent experiments [20–30], indicating the feasibility of this setup. Next, one must adjust the top-gate electric field E_t so that hole chemical potential μ_c lies inside the charge gap of the f layer, $0 < \mu_c < U$, where $\mu_c = \partial\epsilon_c/\partial n_c$ is the chemical potential and ϵ_c is the energy per area of the c layer, U is the charge gap of the f layer, and we measure energy relative to the bottom of the f-layer gap. If correlations are neglected in the c layer,

$$\mu_c = \left(\frac{2\pi e^2}{\epsilon A_M}(\nu_c - 1) + eD\right)d + \epsilon_F(\nu_c) + U, \qquad (1)$$

where the displacement field $D \equiv (E_t + E_b)/2$, ϵ is the background dielectric constant, E_t and E_b are the gate electric fields above the c layer and below the f layer, respectively, d is the separation between WX_2 layers, ν_c is the number of holes per moiré period in the top layer, and $\epsilon_F(\nu_c)$ is the c-layer Fermi energy. Since the total carrier density is related only to the difference in gate fields via the Poisson equation: $4\pi e(1 + \nu_c)/(\epsilon A_M) = E_t - E_b$, ν_c and D can be controlled separately. For a given value of ν_c, μ_c increases monotonically with D and passes through the $(0, U)$ Kondo lattice interval. As illustrated in Fig. 1(c), $\mu_c(D)$ increases with ν_c at fixed D, and both boundaries of the Kondo lattice interval move to smaller D.

Kondo lattice model. Since the on-site repulsion in the f layer, U, greatly exceeds the f-layer hopping and f/c interlayer tunneling amplitudes, within the Kondo lattice regime highlighted in Fig. 1(c), we model the system by a Kondo lattice Hamiltonian that retains only spin degrees of freedom in the f layer:

$$H_{\rm KH} = -t_c \sum_{\langle \boldsymbol{r}\boldsymbol{r}'\rangle} c^\dagger_{\boldsymbol{r}\alpha} c_{\boldsymbol{r}'\alpha} + \frac{J_K}{2} \sum_{\boldsymbol{r}} \boldsymbol{S}_{\boldsymbol{r}} \cdot c^\dagger_{\boldsymbol{r}\alpha} \boldsymbol{\sigma}_{\alpha\beta} c_{\boldsymbol{r}\beta}$$
$$- \mu_c \sum_{\boldsymbol{r}} c^\dagger_{\boldsymbol{r}\alpha} c_{\boldsymbol{r}\alpha} + J_H \sum_{\langle \boldsymbol{r}\boldsymbol{r}'\rangle} \boldsymbol{S}_{\boldsymbol{r}} \cdot \boldsymbol{S}_{\boldsymbol{r}'}. \qquad (2)$$

Here, $\boldsymbol{S}_{\boldsymbol{r}}$ is a spin operator at a triangular-lattice site $\boldsymbol{r}$ in the f layer, $c_{\boldsymbol{r}\alpha}$ annihilates a c-layer electron of spin α at site $\boldsymbol{r}$, and the repeated spin labels are implicitly summed.

We extract the conduction band hopping (t_c) and Kondo coupling (J_K) parameters from self-consistent Hartree-Fock (SCHF) calculations in which the small hybridization, Γ, between the WX_2 layers is temporarily neglected (see Supplemental Material [31] for details). We later reintroduce Γ perturbatively to compute spin-exchange couplings.

Inside the Kondo lattice regime the solutions of the SCHF equations are characterized by a mean-field state that has a small itinerant electron Fermi surface, a fully occupied triangular-lattice [19–22,32] majority-spin local-moment band, and an empty minority-spin local-moment band. SCHF calculations are performed using a continuum moiré model for holes with moiré modulation potentials in the two WX_2 layers that attract holes to lattice sites and are represented by a Fourier expansion $\sum_{\boldsymbol{b}} V_m(\boldsymbol{b})\exp(i\boldsymbol{b}\cdot\boldsymbol{r})$ involving only the first shell of reciprocal lattice vectors $\boldsymbol{b}$ [19]. We use a moiré potential strength $V_m = 30$ meV for the f layer, based on recent experimental estimates [33], and a WSe_2 effective mass $m = 0.35m_e$ [19], where m_e is the mass of an electron. We see in Fig. 1(b) that the c-layer and the minority-spin f-layer mean-field bands are nearly-free-electron-like, with very small band gaps to higher minibands at the zone boundary. This arises due to screening effects that result in approximate cancellation between attraction by the moiré potential and repulsion from the f-layer holes. Despite the small energetic separation between the first and second c-layer minibands, in the Supplemental Material [31] we show that tunneling between the f orbital and the second c band is suppressed, justifying the use of a single-band model for both layers.

The mean-field Hartree potential at each total moiré band filling factor depends on the gate-controlled external displacement field D. The phase boundaries in Fig. 1(c), calculated for the twist angle $\theta = 4.5^\circ$ case, were constructed by identifying the area in the gate-voltage phase space over which the top-layer Fermi level lies in the bottom-layer charge gap. Data for other twist angles are summarized in the Supplemental Material [31].

To estimate the Kondo coupling constant, we perturbatively reintroduce the weak interlayer hybridization, which we take to be momentum independent (see Supplemental Material [31]), via a Schrieffer-Wolff transformation to obtain

$$J_K = 2\Gamma^2\left(\frac{1}{U + E_F^f - E_F^c} - \frac{1}{E_F^f - E_F^c}\right), \tag{3}$$

where E_F^f and E_F^c are the respective Fermi levels. Crucially, we see that J_K can be enhanced with a displacement field that brings the c Fermi level closer to resonance with the upper or lower Hubbard band of the f layer. The estimated Γ is much weaker than the Hubbard gap: For $\theta = 4.5^\circ$, $\Gamma \approx 21.6$ meV and $U \approx 209.06$ meV. As long as the applied displacement field is sufficiently away from the edges of the Kondo lattice regime shown in Fig. 1(c), where the above perturbative formula is valid, the system is well described by a Kondo lattice, and a crossover to a mixed-valence regime is expected closer to the edges. Below, we will show that, for suitable twist angles, this allows gate tuning across a Kondo-screening quantum critical point (KS-QCP).

The Heisenberg exchange coupling, J_H, between the f spins arises both through superexchange $\sim 4t_f^2/U$ between the f-layer spins and via RKKY interactions mediated by the conduction electrons [34]: $J_{\mathrm{RKKY}}(\boldsymbol{r}) = (\nu_c/\sqrt{3}t_c)J_K^2[\mathcal{J}_0(k_F r)\mathcal{Y}_0(k_F r) + \mathcal{J}_1(k_F r)\mathcal{Y}_1(k_F r)]$, where k_F is the conduction electron Fermi momentum and $\mathcal{J}_n$ and $\mathcal{Y}_n$ are Bessel functions of the first and second kinds, respectively [35].

Gate-tuned Kondo physics. The moiré Kondo lattice system has two especially attractive features: (i) It is possible to tune the system between the strong-J_K heavy fermion regime and the more complex weak-J_K regime electrostatically by moving through the phase diagram with gates, and (ii) the intrinsic triangular-lattice geometry frustrates magnetic order and favors the more interesting fractionalized states that are thought to be a strong possibility in the weak-J_K regime. To identify where these states are most likely to occur, we employ a parton [36] mean-field theory [5,37], in which we fractionalize the f-layer spins into neutral spinons $\boldsymbol{S}_{\boldsymbol{r}} = \frac{1}{2}f^\dagger_{\boldsymbol{r}\alpha}\boldsymbol{\sigma}_{\alpha\beta}f_{\boldsymbol{r}\beta}$, which introduces a local-U(1) gauge redundancy $f_{\boldsymbol{r}\alpha} \to e^{i\chi_{\boldsymbol{r}}}f_{\boldsymbol{r}\alpha}$. In an exact treatment this results in an emergent dynamical U(1) gauge field, a_μ, which is approximated as a static background field in the mean-field theory (fluctuations beyond mean field are discussed below where important). Previous parton mean-field studies applied to Kondo systems find spurious finite-temperature phase transitions, which smoothen into crossovers when fluctuations about the mean field are included [5,38,39]. Nevertheless, the zero-temperature quantum phase transition remains sharp [5,39,40] and forms the focus of our following analyses.

In the parton framework, Kondo screening is captured by a nonvanishing value of a (nonlocal) hybridization order parameter $\Delta_{\boldsymbol{r}} = \langle c^\dagger_{\boldsymbol{r}\alpha}f_{\boldsymbol{r}\alpha}\rangle$. For $|\Delta| > 0$ the neutral f spinons hybridize with the charged c electrons to become ordinary charged electrons. When the average background gauge flux a_μ is zero, the system then has both a small Fermi surface of c electrons with weak f character, and a large heavy Fermi surface of f electrons with weak c character; we denote this heavy Fermi liquid phase as FL. By contrast when the hybridization vanishes, $\Delta = 0$, the spinons can form a time-reversal-invariant QSL with a neutral Fermi surface of spinon excitations that coexists with the small Fermi surface of c electrons. We denote this phase as FL* following Ref. [5], which shows how gauge fluctuations beyond mean field give strong non-Fermi-liquid corrections to observable properties of the FL* phase and KS-QCP.

When ring-exchange effects are small, as is the case for the twist angles we consider, the parton mean-field theory has been shown to instead favor mean-field solutions [41] with π emergent magnetic flux per unit cell, which divide unequally between up and down triangular plaquettes (illustrated in the Supplemental Material [31]), spontaneously breaking time-reversal and lattice translation symmetries. The emergent magnetic field gives the spinon bands a net Chern number $C = \pm 1$, to form a chiral spin liquid (CSL). We note that, in this scenario, gauge fluctuations are topologically gapped due to a Chern-Simons term for a_μ induced by the spinon Chern bands. This mean-field prediction is further supported by recent two-dimensional density matrix renormalization group (2D-DMRG) [42] calculations that show that regions of CSL phase arise in triangular-lattice Hubbard models near the Mott transition. Without hybridization ($\Delta = 0$), a CSL of f spins coexists with the c-electron Fermi surface, which we refer to as an anomalous Hall* (AH*) phase. Kondo hybridization ($|\Delta| > 0$), transmits the Berry curvature of the CSL

spins to the hybridized electrons resulting in a time-reversal-symmetry-broken metal with a nonzero (but not quantized) anomalous Hall (AH) conductance.

The parton mean-field phase diagram is shown in Fig. 1(c) (see also Supplemental Material [31]) for twist angle $\theta = 4.5^\circ$. In all regimes sufficiently away from $\nu = 2$ [where a Kondo insulator (KI) arises], AH(*) phases are favored over flux-free FL(*) phases. We have also checked for magnetic mean-field solutions with magnetization, $\langle \boldsymbol{S}_{\boldsymbol{r}} \rangle \neq 0$, forming the 120° pattern favored by the triangular-lattice Heisenberg model, but did not find any regions where AFM order either coexists with or supplants the AH or AH* phases. Crucially, the KS-QCP (here, between AH and AH* phases) is accessible by gate tuning. We estimate the Kondo temperature, the characteristic temperature near which Kondo screening emerges, as $T_K \gtrsim 100$ K using $T_K = \Lambda e^{-1/(2J_K \rho_c)}$ [6], where Λ and ρ_c are the c-electron bandwidth and the density of states at the Fermi level, respectively.

Similar gate-field phase diagrams that include Kondo-screening quantum criticality lines arise over a range of twist angles: $3.5^\circ \lesssim \theta \lesssim 6^\circ$. For larger θ, the f layer is no longer a Mott insulator, and for smaller θ, the Kondo coupling is large compared with t_c, so that only hybridized phases arise. We note that, if desired, the quantum criticality could potentially be accessed at smaller twist angles by suppressing the interlayer tunneling Γ between WX_2 layers, for example, by introducing a hexagonal boron nitride (hBN) spacer layer.

Experimental signatures. Existing measurement techniques for 2D moiré materials offer experimental tests that can both identify the Kondo-screening quantum criticality line and cleanly distinguish among the various proposed QSL and AFM scenarios for the nonhybridized phase. We focus on (i) the entropy density $s(\nu)$, which can be extracted from electrostatic measurements of $\partial\mu/\partial T = -\partial s/\partial \nu$ [43–46], and (ii) electrical (σ) and thermal (κ) longitudinal and Hall conductivities and present detailed parton calculations of these observables in the Supplemental Material [31]. Since thermal transport properties can be challenging to measure, in the Supplemental Material [31] we also describe all-electrical probes of the spinon transport properties of QSL scenarios using a combination of ac measurements and separate contact of the c and f layers.

In each scenario, the c electrons contribute Fermi-liquid-like behavior with $s \sim T$ and $\sigma \sim$ const, which adds to contributions of (neutral) f spinons, with the exception of $\nu = 2$, where we find a featureless KI with activated thermodynamic and transport signatures with gap ≈1.14 meV. In each case, the Kondo hybridization results in a discontinuous jump in electrical conductivities due to the incorporation of f spins into the conducting Fermi sea.

In the AH*-AH scenario favored by our parton calculations, the CSL of f electrons in the AH* phase contributes a quantized thermal Hall conductivity $\kappa_f^{xy} = \frac{\pi^2}{3h} T$ per spin and thermally activated entropy $s \sim e^{-E_g/T}$, with E_g being the spinon gap (Fig. 2). Kondo hybridization produces a quantized jump $|\Delta\sigma^{xy}| = e^2/h$ per spin but smoothly evolving κ^{xy} across the KS-QCP. Note that the previous statements hold for $T \ll E_g$. Alternatively, in a time-reversal-symmetric

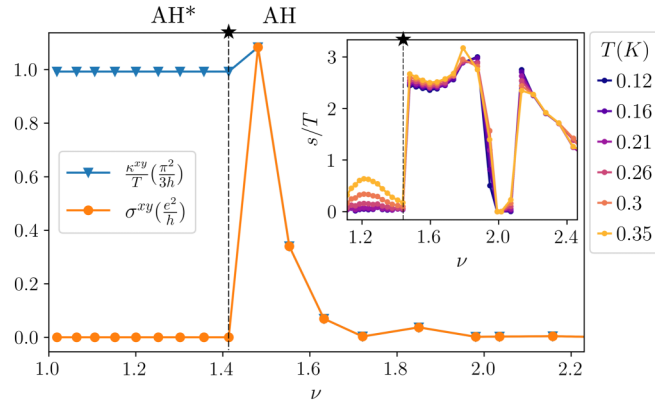

FIG. 2. Thermal (κ^{xy}) and electrical (σ^{xy}) Hall conductivities per spin, calculated using the parton mean-field bands for $\theta = 4.5^\circ$ and $J_K = 22.2$ meV. In the AH* phase, the spinons are in a Chern insulating state with quantized κ^{xy}/T and a gap of ≈0.26 meV at $\nu \approx 1$. σ^{xy} jumps to the κ^{xy}/T value in the AH phase as the spinons acquire electronic character. The inset shows s/T per spin vs ν at temperatures specified by line color. The jump near the KS-QCP is due to effective mass enhancement in the AH phase when the hybridization exceeds the Chern insulator gap.

FL*-FL scenario, the f spinons form a gapless state with a Fermi surface. Here, due to gauge fluctuations beyond the parton mean-field treatment, the spinon entropy contribution varies from non-Fermi-liquid-like $s \sim T^{2/3}$ [5,47] in the FL* phase, marginal FL $s \sim T \ln 1/T$ [40] at the KS-QCP, and an ordinary $s \sim T$ in the FL phase. Lastly, in a more conventional AFM-FL scenario, the spinons are confined in the AFM phase where the f-layer spin waves would contribute $s \sim T^2$, as well as a jump in the $\sim T$ coefficient, Hall density, and conductivity across the KS-QCP. We note that the jump in electrical conductivities across the KS-QCP is expected to be much larger in the AFM-FL and FL*-FL scenarios than in the AH*-AH scenario since the spinons are gapped at the KS-QCP in the latter. Scattering of conduction electrons by spin waves could also lead to characteristic transport signatures, as pointed out recently in Ref. [48]. The experimental signatures discussed so far for the various phases hold in a regime of temperatures much below a quantum critical crossover temperature corresponding to the condensation of Δ, and the quantum critical signatures hold above this temperature [5,40,49].

Discussion. Several extensions of our theoretical analysis could be fruitful avenues for future investigation. Unfrustrated orthorhombic Kondo lattice systems, such as the prototypical heavy fermion compound $CeCoIn_5$, often exhibit superconductivity in the vicinity of the KS-QCP. It remains an open question whether this superconducting tendency persists in frustrated triangular-lattice geometries. Second, large moire unit cells imply large magnetic fluxes per unit cell [50], and therefore significant scalar chirality in local-moment interactions, at relatively weak magnetic field B. These could favor CSL phases [51,52] at finite B even if they were not favored at $B = 0$. The ability to apply a large flux per unit cell could effectively induce orbital emergent gauge fields in the spinon Fermi surface state, leading to quantum oscillatory

phenomena with $1/\kappa B$ periodicity, where κ is an $O(1)$ gauge susceptibility [53]. However, these effects may be challenging to observe in current TMD moiré samples, due to impurity suppression, which so far obscures quantum oscillations even in simple Fermi liquid states. Another promising direction would be to explore the consequences of modifying the electronic structure by imposing relative twists between the two W layers [54–56].

We thank Jie Shan and Qianhui Shi for insightful discussions. A.K. and A.C.P. were supported by the National Science Foundation through the Center for Dynamics and Control of Materials: an NSF MRSEC under Cooperative Agreement No. DMR-1720595. N.C.H. and A.H.M. were supported by the U.S. Department of Energy, Office of Science, Basic Energy Sciences, under Award No. DE-SC0019481. A.C.P. acknowledges support from the Alfred P. Sloan Foundation through a Sloan Research Fellowship. This research was undertaken thanks, in part, to funding from the Max Planck-UBC-UTokyo Center for Quantum Materials and the Canada First Research Excellence Fund, Quantum Materials and Future Technologies Program. The authors acknowledge the Texas Advanced Computing Center (TACC) at The University of Texas at Austin for providing HPC resources that have contributed to the research results reported within this paper.

[1] G. R. Stewart, Heavy-fermion systems, Rev. Mod. Phys. **56**, 755 (1984).
[2] P. Gegenwart, Q. Si, and F. Steglich, Quantum criticality in heavy-fermion metals, Nat. Phys. **4**, 186 (2008).
[3] S. Paschen and Q. Si, Quantum phases driven by strong correlations, Nat. Rev. Phys. **3**, 9 (2021).
[4] P. Coleman, C. Pépin, Q. Si, and R. Ramazashvili, How do Fermi liquids get heavy and die? J. Phys.: Condens. Matter **13**, R723 (2001).
[5] T. Senthil, M. Vojta, and S. Sachdev, Weak magnetism and non-Fermi liquids near heavy-fermion critical points, Phys. Rev. B **69**, 035111 (2004).
[6] S. Doniach, The Kondo lattice and weak antiferromagnetism, Physica B+C (Amsterdam) **91**, 231 (1977).
[7] P. Coleman and N. Andrei, Kondo-stabilised spin liquids and heavy fermion superconductivity, J. Phys.: Condens. Matter **1**, 4057 (1989).
[8] H. V. Löhneysen, A. Rosch, M. Vojta, and P. Wölfle, Fermi-liquid instabilities at magnetic quantum phase transitions, Rev. Mod. Phys. **79**, 1015 (2007).
[9] I. Martin and C. D. Batista, Itinerant Electron-Driven Chiral Magnetic Ordering and Spontaneous Quantum Hall Effect in Triangular Lattice Models, Phys. Rev. Lett. **101**, 156402 (2008).
[10] Y. Kato, I. Martin, and C. D. Batista, Stability of the Spontaneous Quantum Hall State in the Triangular Kondo-Lattice Model, Phys. Rev. Lett. **105**, 266405 (2010).
[11] L. Zou, H. C. Po, A. Vishwanath, and T. Senthil, Band structure of twisted bilayer graphene: Emergent symmetries, commensurate approximants, and Wannier obstructions, Phys. Rev. B **98**, 085435 (2018).
[12] H. C. Po, L. Zou, T. Senthil, and A. Vishwanath, Faithful tight-binding models and fragile topology of magic-angle bilayer graphene, Phys. Rev. B **99**, 195455 (2019).
[13] Z. Song, Z. Wang, W. Shi, G. Li, C. Fang, and B. A. Bernevig, All Magic Angles in Twisted Bilayer Graphene are Topological, Phys. Rev. Lett. **123**, 036401 (2019).
[14] J. Ahn, S. Park, and B.-J. Yang, Failure of Nielsen-Ninomiya Theorem and Fragile Topology in Two-Dimensional Systems with Space-Time Inversion Symmetry: Application to Twisted Bilayer Graphene at Magic Angle, Phys. Rev. X **9**, 021013 (2019).
[15] A. Ramires and J. L. Lado, Emulating Heavy Fermions in Twisted Trilayer Graphene, Phys. Rev. Lett. **127**, 026401 (2021).
[16] A. Dalal and J. Ruhman, Orbitally selective Mott phase in electron-doped twisted transition metal-dichalcogenides: A possible realization of the Kondo lattice model, Phys. Rev. Research **3**, 043173 (2021).
[17] We ignore Γ-valley bands here for reasons detailed in the Supplemental Material [31].
[18] D. Xiao, G.-B. Liu, W. Feng, X. Xu, and W. Yao, Coupled Spin and Valley Physics in Monolayers of MoS_2 and other Group-VI Dichalcogenides, Phys. Rev. Lett. **108**, 196802 (2012).
[19] F. Wu, T. Lovorn, E. Tutuc, and A. H. MacDonald, Hubbard Model Physics in Transition Metal Dichalcogenide Moiré Bands, Phys. Rev. Lett. **121**, 026402 (2018).
[20] Y. Tang, L. Li, T. Li, Y. Xu, S. Liu, K. Barmak, K. Watanabe, T. Taniguchi, A. H. MacDonald, J. Shan, and K. F. Mak, Simulation of Hubbard model physics in WSe_2/WS_2 moiré superlattices, Nature (London) **579**, 353 (2020).
[21] E. C. Regan, D. Wang, C. Jin, M. I. B. Utama, B. Gao, X. Wei, S. Zhao, W. Zhao, Z. Zhang, K. Yumigeta, M. Blei, J. D. Carlström, K. Watanabe, T. Taniguchi, S. Tongay, M. F. Crommie, A. Zettl, and F. Wang, Mott and generalized Wigner crystal states in WSe_2/WS_2 moiré superlattices, Nature (London) **579**, 359 (2020).
[22] L. Wang, E.-M. Shih, A. Ghiotto, L. Xian, D. A. Rhodes, C. Tan, M. Claassen, D. M. Kennes, Y. Bai, B. Kim, K. Watanabe, T. Taniguchi, X. Zhu, J. C. Hone, Á. Rubio, A. N. Pasupathy, and C. R. Dean, Correlated electronic phases in twisted bilayer transition metal dichalcogenides, Nat. Mater. **19**, 861 (2020).
[23] Y. Xu, S. Liu, D. A. Rhodes, K. Watanabe, T. Taniguchi, J. Hone, V. Elser, K. F. Mak, and J. Shan, Correlated insulating states at fractional fillings of moiré superlattices, Nature (London) **587**, 214 (2020).
[24] C. Jin, Z. Tao, T. Li, Y. Xu, Y. Tang, J. Zhu, S. Liu, K. Watanabe, T. Taniguchi, J. C. Hone, L. Fu, J. Shan, and K. F. Mak, Stripe phases in WSe_2/WS_2 moiré superlattices, Nat. Mater. **20**, 940 (2021).
[25] T. Li, J. Zhu, Y. Tang, K. Watanabe, T. Taniguchi, V. Elser, J. Shan, and K. F. Mak, Charge-order-enhanced capacitance in semiconductor moiré superlattices, Nat. Nanotechnol. **16**, 1068 (2021).
[26] H. Li, S. Li, M. H. Naik, J. Xie, X. Li, E. C. Regan, D. Wang, W. Zhao, K. Yumigeta, M. Blei, T. Taniguchi, K. Watanabe, S. Tongay, A. Zettl, S. G. Louie, M. F. Crommie, and F. Wang, Imaging local discharge cascades for correlated electrons in WS_2/WSe_2 moiré superlattices, Nat. Phys. **17**, 1114 (2021).

[27] X. Huang, T. Wang, S. Miao, C. Wang, Z. Li, Z. Lian, T. Taniguchi, K. Watanabe, S. Okamoto, D. Xiao, S.-F. Shi, and Y.-T. Cui, Correlated insulating states at fractional fillings of the WS_2/WSe_2 moiré lattice, Nat. Phys. **17**, 715 (2021).

[28] T. Li, S. Jiang, L. Li, Y. Zhang, K. Kang, J. Zhu, K. Watanabe, T. Taniguchi, D. Chowdhury, L. Fu, J. Shan, and K. F. Mak, Continuous Mott transition in semiconductor moiré superlattices, Nature (London) **597**, 350 (2021).

[29] A. Ghiotto, E.-M. Shih, G. Pereira, D. A. Rhodes, B. Kim, J. Zang, A. J. Millis, K. Watanabe, T. Taniguchi, J. C. Hone, L. Wang, C. R. Dean, and A. N. Pasupathy, Quantum criticality in twisted transition metal dichalcogenides, Nature (London) **597**, 345 (2021).

[30] T. Li, S. Jiang, B. Shen, Y. Zhang, L. Li, Z. Tao, T. Devakul, K. Watanabe, T. Taniguchi, L. Fu, J. Shan, and K. F. Mak, Quantum anomalous Hall effect from intertwined moiré bands, Nature (London) **600**, 641 (2021).

[31] See Supplemental Material at http://link.aps.org/supplemental/10.1103/PhysRevB.106.L041116 for details of the self-consistent Hartree-Fock calculation and parton mean-field calculation, including results for different twist angles. We also present a discussion of transport properties near the Kondo-screening quantum critical point, including Refs. [57–65].

[32] N. C. Hu and A. H. MacDonald, Competing magnetic states in transition metal dichalcogenide moiré materials, Phys. Rev. B **104**, 214403 (2021).

[33] S. Shabani, D. Halbertal, W. Wu, M. Chen, S. Liu, J. Hone, W. Yao, D. N. Basov, X. Zhu, and A. N. Pasupathy, Deep moiré potentials in twisted transition metal dichalcogenide bilayers, Nat. Phys. **17**, 720 (2021).

[34] D. N. Aristov, Indirect RKKY interaction in any dimensionality, Phys. Rev. B **55**, 8064 (1997).

[35] To smoothly interpolate to the strong-coupling regime, $J_{\mathrm{RKKY}} \sim J_K$ when $J_K \gg t_c$, in calculations we divide this perturbative formula by a factor $\sqrt{1+(J_K/t_c)^2}$, which produces the correct strong- and weak-coupling asymptotics.

[36] Sometimes indelicately referred to as "slave spin.".

[37] A. C. Hewson, *The Kondo Problem to Heavy Fermions*, Cambridge Studies in Magnetism (Cambridge University Press, Cambridge, 1997), Vol. 2.

[38] P. Coleman, New approach to the mixed-valence problem, Phys. Rev. B **29**, 3035 (1984).

[39] P. Coleman, *Introduction to Many-Body Physics* (Cambridge University Press, Cambridge, 2015).

[40] T. Senthil, Theory of a continuous Mott transition in two dimensions, Phys. Rev. B **78**, 045109 (2008).

[41] O. I. Motrunich, Variational study of triangular lattice spin-1/2 model with ring exchanges and spin liquid state in κ–$(ET)_2Cu_2(CN)_3$, Phys. Rev. B **72**, 045105 (2005).

[42] A. Szasz, J. Motruk, M. P. Zaletel, and J. E. Moore, Chiral Spin Liquid Phase of the Triangular Lattice Hubbard Model: A Density Matrix Renormalization Group Study, Phys. Rev. X **10**, 021042 (2020).

[43] A. Y. Kuntsevich, Y. Tupikov, V. Pudalov, and I. Burmistrov, Strongly correlated two-dimensional plasma explored from entropy measurements, Nat. Commun. **6**, 7298 (2015).

[44] N. Hartman, C. Olsen, S. Lüscher, M. Samani, S. Fallahi, G. C. Gardner, M. Manfra, and J. Folk, Direct entropy measurement in a mesoscopic quantum system, Nat. Phys. **14**, 1083 (2018).

[45] A. Rozen, J. M. Park, U. Zondiner, Y. Cao, D. Rodan-Legrain, T. Taniguchi, K. Watanabe, Y. Oreg, A. Stern, E. Berg, P. Jarillo-Herrero, and S. Ilani, Entropic evidence for a Pomeranchuk effect in magic-angle graphene, Nature (London) **592**, 214 (2021).

[46] Y. Saito, F. Yang, J. Ge, X. Liu, T. Taniguchi, K. Watanabe, J. Li, E. Berg, and A. F. Young, Isospin Pomeranchuk effect in twisted bilayer graphene, Nature (London) **592**, 220 (2021).

[47] P. A. Lee and N. Nagaosa, Gauge theory of the normal state of high-T_c superconductors, Phys. Rev. B **46**, 5621 (1992).

[48] A. L. Chernyshev and O. A. Starykh, Roller Coaster in a Flatland: Magnetoresistivity in Eu-Intercalated Graphite, Phys. Rev. X **12**, 021010 (2022).

[49] S. Sachdev, *Quantum Phase Transitions* (Cambridge University Press, Cambridge, 2011).

[50] C. R. Dean, L. Wang, P. Maher, C. Forsythe, F. Ghahari, Y. Gao, J. Katoch, M. Ishigami, P. Moon, M. Koshino, T. Taniguchi, K. Watanabe, K. L. Shepard, J. Hone, and P. Kim, Hofstadter's butterfly and the fractal quantum Hall effect in moiré superlattices, Nature (London) **497**, 598 (2013).

[51] W.-J. Hu, S.-S. Gong, and D. N. Sheng, Variational Monte Carlo study of chiral spin liquid in quantum antiferromagnet on the triangular lattice, Phys. Rev. B **94**, 075131 (2016).

[52] A. Wietek and A. M. Läuchli, Chiral spin liquid and quantum criticality in extended $S = \frac{1}{2}$ Heisenberg models on the triangular lattice, Phys. Rev. B **95**, 035141 (2017).

[53] O. I. Motrunich, Orbital magnetic field effects in spin liquid with spinon Fermi sea: Possible application to κ–$(ET)_2Cu_2(CN)_3$, Phys. Rev. B **73**, 155115 (2006).

[54] F. Wu, T. Lovorn, E. Tutuc, I. Martin, and A. H. MacDonald, Topological Insulators in Twisted Transition Metal Dichalcogenide Homobilayers, Phys. Rev. Lett. **122**, 086402 (2019).

[55] H. Pan, F. Wu, and S. Das Sarma, Band topology, Hubbard model, Heisenberg model, and Dzyaloshinskii-Moriya interaction in twisted bilayer WSe_2, Phys. Rev. Research **2**, 033087 (2020).

[56] J. Zang, J. Wang, J. Cano, and A. J. Millis, Hartree-Fock study of the moiré Hubbard model for twisted bilayer transition metal dichalcogenides, Phys. Rev. B **104**, 075150 (2021).

[57] J. Xiao, M. Long, X. Li, Q. Zhang, H. Xu, and K. S. Chan, Effects of van der Waals interaction and electric field on the electronic structure of bilayer MoS_2, J. Phys.: Condens. Matter **26**, 405302 (2014).

[58] K. F. Mak, C. Lee, J. Hone, J. Shan, and T. F. Heinz, Atomically Thin MoS_2: A New Direct-Gap Semiconductor, Phys. Rev. Lett. **105**, 136805 (2010).

[59] A. Splendiani, L. Sun, Y. Zhang, T. Li, J. Kim, C.-Y. Chim, G. Galli, and F. Wang, Emerging photoluminescence in monolayer MoS_2, Nano Lett. **10**, 1271 (2010).

[60] Y. Zhang, T.-R. Chang, B. Zhou, Y.-T. Cui, H. Yan, Z. Liu, F. Schmitt, J. Lee, R. Moore, Y. Chen, H. Lin, H.-T. Jeng, S.-K. Mo, Z. Hussain, A. Bansil, and Z.-X. Shen, Direct observation of the transition from indirect to direct bandgap in atomically thin epitaxial $MoSe_2$, Nat. Nanotechnol. **9**, 111 (2014).

[61] H. C. P. Movva, T. Lovorn, B. Fallahazad, S. Larentis, K. Kim, T. Taniguchi, K. Watanabe, S. K. Banerjee, A. H. MacDonald, and E. Tutuc, Tunable $\Gamma - K$ Valley Populations in Hole-Doped Trilayer WSe_2, Phys. Rev. Lett. **120**, 107703 (2018).

[62] P. V. Nguyen, N. C. Teutsch, N. P. Wilson, J. Kahn, X. Xia, A. J. Graham, V. Kandyba, A. Giampietri, A. Barinov, G.

Constantinescu, N. C. Yeung, N. Hine, X. Xu, D. H. Cobden, and N. R. Wilson, Visualizing electrostatic gating effects in two-dimensional heterostructures, Nature (London) **572**, 220 (2019).

[63] E. J. Sie, T. Rohwer, C. Lee, and N. Gedik, Time-resolved XUV ARPES with tunable 24–33 eV laser pulses at 30 meV resolution, Nat. Commun. **10**, 3535 (2019).

[64] L. B. Ioffe and A. I. Larkin, Gapless fermions and gauge fields in dielectrics, Phys. Rev. B **39**, 8988 (1989).

[65] E. E. Aldape, T. Cookmeyer, A. A. Patel, and E. Altman, Solvable theory of a strange metal at the breakdown of a heavy Fermi liquid, Phys. Rev. B **105**, 235111 (2022).